Structure and Properties of La$_{0.4}$Sr$_{0.4}$TiO$_3$ Ceramics for Use as Anode Materials in Solid Oxide Fuel Cells

Dragos Neagu* and John T. S. Irvine

School of Chemistry, University of St. Andrews, Fife, Scotland, KY16 9ST

Received May 28, 2010. Revised Manuscript Received July 20, 2010

In this work, La$_{0.4}$Sr$_{0.4}$TiO$_3$-based ceramics intended for use as anode materials in solid oxide fuel cells were investigated. The material was found to preserve its cubic structure throughout testing across a range of conditions, although slight signs of phase segregation were also identified under extreme conditions. The thermal expansion coefficient measured on differently processed samples predicts a good thermomechanical compatibility with yttria-stabilized zirconia (YSZ). Conductivity measurements indicated that the material exhibits a fast surface reduction, unlike the bulk reduction, which progresses very slowly. An increase of the prereduction temperature was found to significantly increase the extent of the reduction and, therefore, the conductivity. Samples sintered under a 5% H$_2$/Ar flow, at 1400 °C, showed high conductivities of up to 96 S cm^{-1} at 880 °C and oxygen partial pressures of $p_{O_2} = 10^{-20}$ atm. Correlations between the oxygen deficiency, conductivity, porosity, reduction temperature, and cell parameter are also presented. An equation that accounts for the expansion of the cell parameter on reduction has been adapted from the literature and is discussed.

1. Introduction

Solid oxide fuel cells (SOFCs) are electrochemical devices that produce electricity directly from the oxidation of fuels. Because of their fuel flexibility and very high potential efficiency, they are regarded as one of the most attractive solutions for clean, future power generation.[1] Most of the difficulties faced in the improvement of the current state-of-the-art SOFCs are related to finding a suitable replacement for the current anode, the Ni-YSZ cermet. Although this anode exhibits excellent catalytic activity and current collection, it also suffers from serious limitations, such as nickel sintering, carbon deposition, sulfur poisoning,[2] or low tolerance to redox cycles, which are usually associated with its characteristic two-phase architecture. Therefore, several materials and approaches are being considered to address these problems and find a suitable all-ceramic anode. A viable anode material should fulfill some basic requirements, such as good chemical and mechanical stability under SOFC operating conditions, high electronic and ionic conductivity over a wide range of oxygen partial pressures (p_{O_2}), good chemical and thermal compatibility with electrolyte and interconnect materials, high surface exchange kinetics, and good catalytic properties for the anode reactions.[3] Because of these demanding requirements, it is often necessary to reach a compromise in physical and chemical properties, usually in terms of stability and electrical properties.[4]

In this context, much of the effort has been directed toward perovskite materials (ABO$_3$), because of the general stability and doping flexibility of this system.[1,4−6] Perovskite structures are also of interest because they can incorporate cations with multiple oxidation states, which facilitate electrocatalytic processes and provide mechanisms for electronic conductivity. Several doping scenarios have been envisaged and investigated to manipulate the structure, defect chemistry, and, therefore, the properties of perovskites. Among some of the doping strategies that have yielded materials with unique features, we mention perovskites that exhibit oxygen excess (ABO$_{3+\delta}$), oxygen deficiency (ABO$_{3-\delta}$), and A-site deficiency (A$_{1-x}$BO$_3$), where A and B denote the sites of the perovskite and each can be occupied by one or more suitable cations. Some of these features will be briefly described and discussed below for the case of titanates (B = Ti).

Among the numerous other perovskite systems that have been explored, those containing titanium continue to attract attention, because titanium remains mixed-valent Ti^{4+}/Ti^{3+} in the reducing atmosphere at the anode, and this redox couple can accept electrons from a hydrocarbon or H$_2$, thus promoting their dissociation.[1] Because the formation of Ti^{3+} is favored by the reducing conditions, the atmosphere used during the sintering stage plays a crucial role in determining the final properties of these materials. Usually, the higher the sintering temperature

---

*Author to whom correspondence should be addressed. E-mail: dn67@st-andrews.ac.uk.

(1) Goodenough, J. B.; Huang, Y. *J. Power Sources* **2007**, *173*, 1–10.
(2) Matsuzaki, Y.; Yasuda, I. *Solid State Ionics* **2000**, *132*, 261–269.
(3) Minh, N. *Solid State Ionics* **2004**, *174*, 271–277.
(4) Ishihara, T. *Perovskite Oxide for Solid Oxide Fuel Cells*; Springer: New York and London, 2008.
(5) Atkinson, A.; Barnett, S.; Gorte, R. J.; Irvine, J. T. S.; McEvoy, A. J.; Mogensen, M.; Singhal, S. C.; Vohs, J. *Nat. Mater.* **2004**, *3*, 17–27.
(6) Fergus, J. W. *Solid State Ionics* **2006**, *177*, 1529–1541.

and the stronger the reducing conditions, the higher the final conductivity will be, because of the higher concentration of Ti^{4+}/Ti^{3+} couples created. For example, lanthanum-doped strontium titanates ($Sr_{1-x}La_xTiO_{3+\delta}$) exhibit conductivities of $1-16$ S cm^{-1}, when sintered in air and measured at 1000 °C and low p_{O_2}, and $80-360$ S cm^{-1}, when sintered in H_2 at 1650 °C and measured under the same conditions.[7] However, the compositions sintered in air have been shown to accommodate extra oxygen between the perovskite blocks, which accounts for their oxygen-rich structure. For $\delta < 0.167$, these extended defects become disordered and the perovskite is more easily reduced.[8] However, the ionic conductivity remains low and does not sustain a good catalytic activity,[9] despite the promising results in terms of stability, compatibility with YSZ,[7] or sulfur poisoning.[10]

The oxygen-deficient compositions can be obtained by doping on the B-site with a cation of lower valence than the valence of the nominal B-site ion or by reducing a stoichiometric composition. The first approach led to the discovery of the compound with the highest known oxide ionic conductivity, $La_{1-x}Sr_xGa_{1-y}Mg_yO_{3-\delta}$.[11,12]

A-site deficiency has been recently used in various systems to prepare materials that are suitable for SOFC anodes. $Sr_{1-(3x/2)}La_xTiO_3$ compositions sintered in air have been shown to exhibit conductivity values up to 7 S cm^{-1} upon reduction at 930 °C and $p_{O_2} = 10^{-20}$ atm.[13,14] The optimized composition of $Sr_{0.86}Y_{0.08}TiO_{3-\delta}$ presents a conductivity of 82 S cm^{-1} at $p_{O_2} = 10^{-19}$ atm and 800 °C, after being prereduced in 7% H_2/Ar at 1400 °C,[15,16] which does not greatly increase when further doped on the B-site.[17] The effect of A-site deficiency has also been found to increase the electronic conduction of $Sr_{1-x}TiO_3$ under reducing conditions.[18] However, the increase is not significant and phase segregation was also observed.[19]

In this paper, we report on a more-extensive study on the synthesis, structure, and properties of the $x = 0.4$ composition belonging to the series $Sr_{1-(3x/2)}La_xTiO_3$. Experiments were carried out to better understand the correlation between electronic conductivity and oxygen deficiency in these compounds.

Previous work carried out by Slater et al.[13] recommended this material as a possible candidate for use as anode material in SOFCs, because of its tolerance to redox cycles and sufficiently high conductivity values.[5] Also, this material is easily synthesized in air, which makes it attractive from a manufacturing point of view. Although, in this series, the conductivity of the samples increased with increasing La content up to $x = 0.67$, the $x = 0.4$ composition was chosen for this study, based on structural and phase-purity considerations. It has been reported that the phase purity of the samples with $x > 0.4$ is questionable, because very small amounts of pyrochlore phase were found in these compositions, although it is not clear whether the synthesis method or phase stability itself is the cause.[20] Also, because of the increased concentration of the vacancies on the A-site as x increases, cation-vacancy ordering has been shown to occur for compositions with $x \geq 0.4$.[21] For $0 < x < 0.4$, the structure of the materials is cubic, followed by a tetragonal distortion for $0.4 < x < 0.55$, leading to an orthorhombic structure for $0.55 < x < 0.67$, for temperatures higher than 300 K.[22] As shown previously for the doped titanates containing oxygen excess,[8] the compositional domain where ordering occurs should be avoided, because it can inhibit the reduction of the material. Moreover, the high A-site deficiency of the $x = 0.4$ composition has been suggested to positively influence the removal of oxygen from the structure by limiting the intrinsic Schottky defect concentration.[4]

2. Experimental Section

$La_{0.4}Sr_{0.4}TiO_3$ (LST) ceramics have been prepared via solid-state synthesis using high-purity La_2O_3 (dried at 800 °C), $SrCO_3$, and TiO_2 (both dried at 300 °C). The dried powders were mixed in the corresponding amounts in a beaker, using acetone. An ultrasonic probe was used to produce a fine suspension of the starting powder mixture. The acetone was evaporated under stirring, and the powder was calcined at 1000 °C for 12 h. The calcined powder was then ball-milled, pressed into pellets, and fired at 1400 °C for 10 h. The obtained pellets were reground, mixed with pore formers (glassy carbon and/or graphite), and fired slowly to $1450-1500$ °C for $7-10$ h to obtain porous ceramics. Experiments that required a reducing environment were performed in a tubular furnace under a continuous 5% H_2/Ar flow.

The crystal structure of the samples was analyzed using X-ray diffraction (XRD) performed on either a Stoe Stadi transmission diffractometer (Cu Kα_1 radiation) or a Philips PW 1710 reflection diffractometer (Cu Kα_1, Kα_2 radiation). The obtained XRD patterns were analyzed with STOE Win XPOW software to determine the crystal structure and the cell parameter. Some of the cell parameters were also refined using the Rietveld method (using FullProf software).

A JEOL JSM-5600 scanning electron microscopy (SEM) system was used to analyze the microstructure of the pellets. Energy-dispersive X-ray analysis was performed to confirm the stoichiometry of the samples.

(7) Marina, O. A.; Canfield, N. L.; Stevenson, J. W. *Solid State Ionics* **2002**, *149*, 21–28.

(8) Ruiz-Morales, J. C.; Canales-Vázquez, J.; Savaniu, C.; Marrero-López, D.; Zhou, W.; Irvine, J. T. S. *Nature* **2006**, *439*, 568–571.

(9) Canales-Vazquez, J.; Tao, S.; Irvine, J. T. S. *Solid State Ionics* **2003**, *159*, 159–165.

(10) Mukundan, R.; Brosha, E. L.; Garzon, F. H. *Electrochem. Solid-State Lett.* **2004**, *7*, A5.

(11) Ishihara, T.; Matsuda, H.; Azmi bin Bustam, M.; Takita, Y. *Solid State Ionics* **1996**, *86–88*, 197–201.

(12) Slater, P. R.; Irvine, J. T. S.; Ishihara, T.; Takita, Y. *J. Solid State Chem.* **1998**, *139*, 135–143.

(13) Slater, P. R.; Fagg, D. P.; Irvine, J. T. S. *J. Mater. Chem.* **1997**, *7*, 2495–2498.

(14) Savaniu, C.; Irvine, J. T. S. *J. Mater. Chem.* **2009**, *19*, 8119–8128.

(15) Hui, S.; Petric, A. *J. Eur. Ceram. Soc.* **2002**, *22*, 1673–1681.

(16) Hui, S.; Petric, A. *J. Electrochem. Soc.* **2002**, *149*, J1.

(17) Hui, S.; Petric, A. *Mater. Res. Bull.* **2002**, *37*, 1215–1231.

(18) Kolodiazhnyi, T.; Petric, A. *J. Electroceram.* **2005**, *15*, 5–11.

(19) Blennow, P.; Hansen, K. K.; Reine Wallenberg, L.; Mogensen, M. *Electrochim. Acta* **2006**, *52*, 1651–1661.

(20) Balachandran, U.; Eror, N. G. *J. Am. Ceram. Soc.* **1981**, *64*, c-75–c-76.

(21) Battle, P.; Bennett, J. E.; Sloan, J.; Tilley, R. J. D.; Vente, J. F. *J. Solid State Chem.* **2000**, *149*, 360–369.

(22) Howard, C.; Lumpkin, G.; Smith, R.; Zhang, Z. *J. Solid State Chem.* **2004**, *177*, 2726–2732.

Thermogravimetric analysis was performed using a Netzsch Model STA 449C instrument that was equipped with Proteus thermal analysis software.

The thermal expansion of the pellets in various atmospheres was investigated using a Netzsch Model DIL 402 C instrument that was equipped with Proteus analysis software.

The DC conductivity of the samples was measured using either a conventional four-probe DC technique or a van der Pauw setup.[23] Both setups consisted of a vertical furnace with controlled atmosphere, equipped with zirconia sensors to monitor the p_{O_2} data. A continuous 5% H_2/Ar flow was used to achieve low p_{O_2} values. The p_{O_2} value can also be increased by allowing air into the furnace through a controlled leak. The difference between the two setups resides in the principle of measuring the conductivity and, therefore, the placement of the metallic contacts on the samples. For the four-probe method, four platinum foil contacts were attached parallel to each other on the surface of the pellets, using platinum paste. For the van der Pauw measurement, four gold mesh contacts were attached at the periphery of the sample, using gold paste. The contacts were consolidated by firing at 800−900 °C for 1 h.

3. Results and Discussion

3.1. Phase Development and Microstructure. Powder XRD confirmed that $La_{0.4}Sr_{0.4}TiO_3$ (LST) forms a single-phase cubic structure ($Pm\bar{3}m$) when sintered either in air or 5% H_2/Ar at 1400 °C (see Figure 1), which is consistent with a random distribution of the vacancies, as discussed earlier. The cell parameters obtained for the two situations can be compared in Table 1. The cell parameter for the sample sintered in reducing environment is larger than the cell parameter of the sample sintered in air. This is due to (i) the higher volume of the Ti^{3+} ions (compared to the Ti^{4+} ions) that form under reducing conditions and (ii) the removal of oxygen anions from the lattice that accompanies this reduction. Generally, a lattice that has a lower content of oxygen than the stoichiometric value will tend to expand, because of the decrease of the Coulombic forces in the unit cell. The expansion of the unit cell was also observed when reducing samples that had previously been sintered in air. The expansion of the unit cell also will be addressed in a quantitative manner toward the end of this paper.

The type of atmosphere used upon sintering does not affect only the cell parameter; it also seems to have a strong influence on the microstructure of the samples, as can be seen from Table 2. The sample sintered in air develops a microstructure with large well-defined polygonal grains ∼60−80 μm in diameter. The sample sintered at lower p_{O_2} (in argon) shows smaller polygonal grains that do not exceed 20−30 μm in diameter. The sample sintered in a very reducing environment (5% H_2/Ar) has an even smaller grain size with many curved grain boundaries and some pores as well. The different microstructure is also reflected in the relative densities calculated for the considered samples, showing a decrease of the relative density with decreasing p_{O_2}. Also note that the samples sintered in air and argon have a dark green color, while the sample that was sintered under extremely
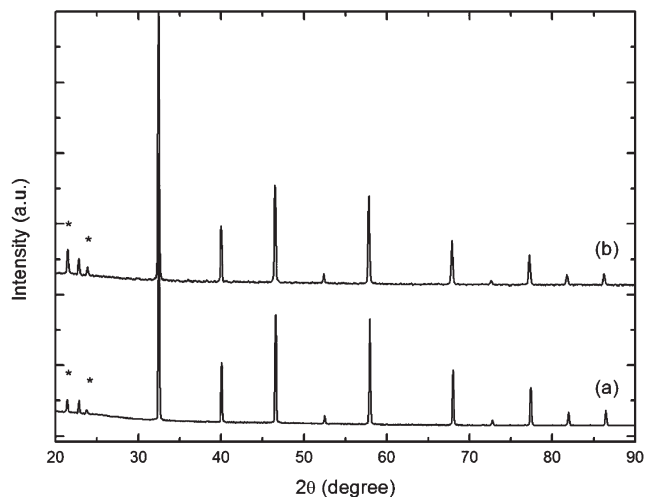
(23) Kasl, C.; Hoch, M. J. R. *Rev. Sci. Instrum.* **2005**, *76*, 033907.

Figure 1. Powder X-ray diffraction (XRD) patterns for powders sintered (a) in air and (b) in 5% H_2/Ar.

Table 1. Refined Cell Parameters for $La_{0.4}Sr_{0.4}TiO_3$ (LST) Ceramics Sintered in Air and 5% H_2/Ar

sintering conditions	air	5% H_2/Ar
temperature (°C)	1400	1400
dwell time (h)	12	12
heating/cooling rate (°C/min)	5/5	5/5
space group	$Pm\bar{3}m$	$Pm\bar{3}m$
cell parameter (Å)	3.8891(2)	3.9009(3)

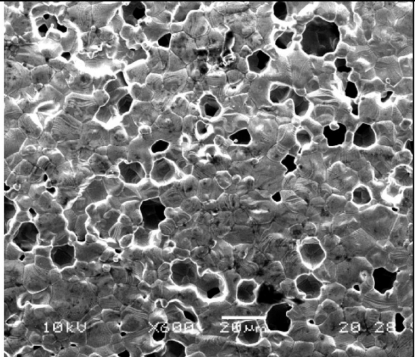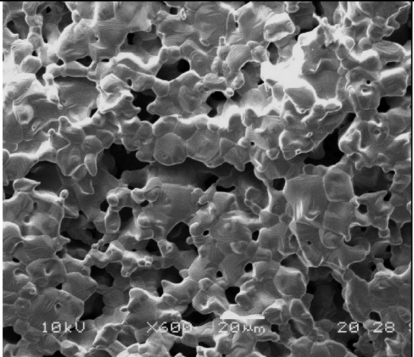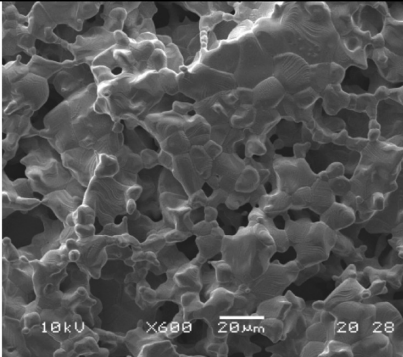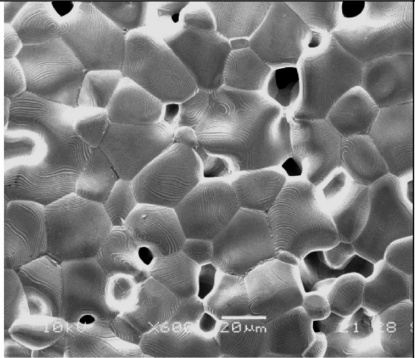**Table 2. Influence of the Sintering Atmosphere on the Microstructure of LST Dense Pellets[a]**
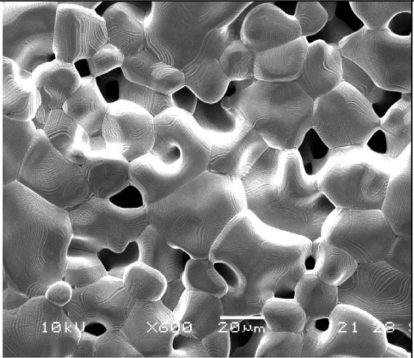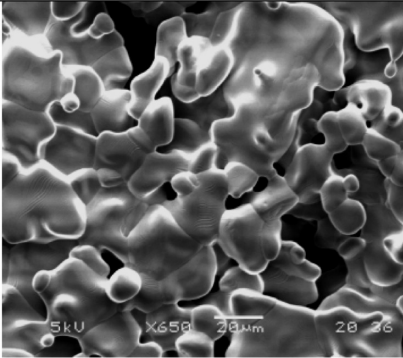
Air	Argon	5%H_2/Ar
1400°C, 12h, (ρ_r~96%)	1400°C, 12h, (ρ_r~93%)	1400°C, 12h, (ρ_r~90%)

[a] At 900 °C, the p_{O_2} value of Ar is ∼$10^{-3.5}$ atm, and the p_{O_2} value of 5% H_2/Ar is ∼10^{-20} atm.

reducing conditions is black, because of the increased concentration of the charge carriers (electrons).

Since anodes used in SOFCs must be porous, it is interesting to study the possibilities of obtaining porous LST ceramics. To obtain these ceramics, pore formers (PFs) were used. In this work, a mixture of equal quantities of glassy carbon and graphite was used in this scope. This type of mixture was found to provide the best porosity, in terms of pore distribution and size. Because LST tends to densify very well in air, thus yielding pellets with low porosity, and the amount of pore formers that can be added is limited by the mechanical stability of the pellets before firing, another method was proposed to achieve pellets with higher porosity. Powder of presintered LST was mixed with calcined powder and pore formers in different ratios and fired in air at 1450−1500 °C for 7−12 h. The influence of the percentage of the added PFs and already-sintered LST on the microstructure and relative density is shown in Table 3 and Figure 2, respectively.

Table 3. Array of Microstructures of the LST Pellets Sintered in Air and Containing Various Amounts of Presintered LST and Pore Formers

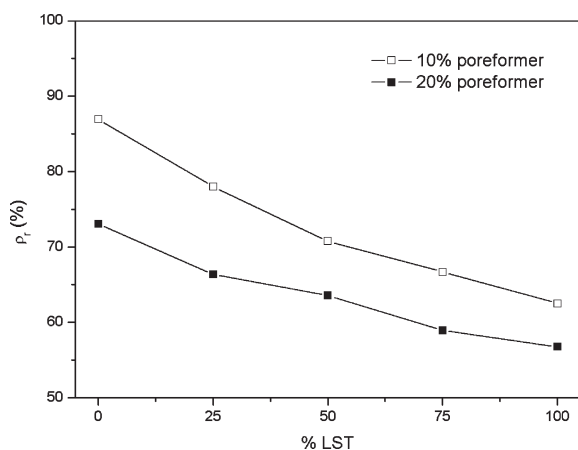| | 0% pre-sintered LST | 50% pre-sintered LST | 100% pre-sintered LST |

Figure 2. Relative densities obtained for samples sintered in air and initially containing a mixture of calcined powder, presintered LST (% LST), and pore formers (PFs).

Obtaining porous pellets via sintering in 5% H_2/Ar and using the pore formers mentioned above was found to be impossible. The XRD pattern of such a pellet does not show cubic symmetry, probably because of the extremely reducing environment in the pellet due to the carbon. However, perhaps a different approach could be found to produce porous structures under these conditions.

3.2. Stability. The cubic perovskite phase was found to be very stable in air, in terms of crystal structure and microstructure. However, it is more important to evaluate its stability in a reducing atmosphere, because this material is intended for use at the anode side of the fuel cell. The XRD patterns show that reducing the perovskite phase at temperatures in the range of 1100−1300 °C does not affect its symmetry: it only affects the position of the peaks that shift to higher *d*-spacing values (see Figure 3). However, signs of possible stability issues have been observed via SEM. It seems that, after reducing the material at high temperatures or after prolonged testing in 5% H_2/Ar, some sub-micron crystals are formed (see Table 4). This might be due to the locally occurring inhomogeneities associated with solid-state synthesis; however, there is no evidence of submicrometer-sized crystals in unreduced samples. It has not been possible to identify the nature of these crystals so far, because they are very small and therefore evade typical structure analysis methods such as energy-dispersive X-ray analysis (EDX) or XRD. Although their presence may cause concern regarding the stability of the material in a reducing atmosphere, they could also bring benefits by acting as catalytic centers or promoting electrochemical reactions. Also note that the general appearance of the grains seems to be retained, even after prolonged testing, so the material could prove to be sufficiently stable under working conditions. It is most likely that the exsolution of these submicrometer-sized crystals is linked to the inability of the A-site-deficient lattice to accommodate the degree of oxygen deficiency induced on reduction and, hence, the small particles are TiO_2 or a reduced titanium oxide. The presence, shape, size and distribution of these exsolutions seems to indicate an association of the strontium and oxygen vacancies in pairs, $(V''_{Sr}V^{\bullet\bullet}_O)$, as it has been
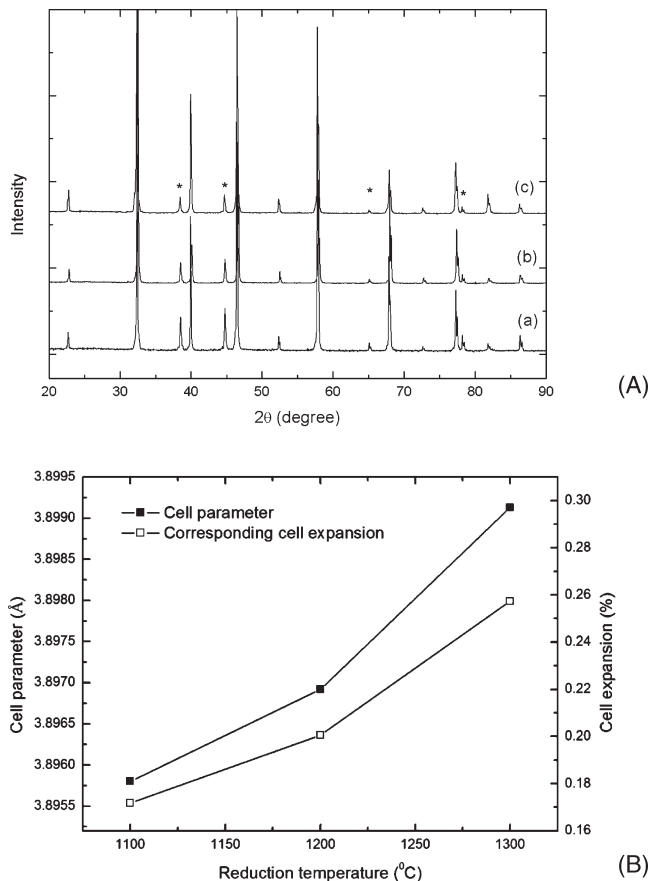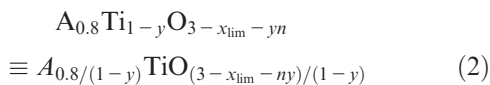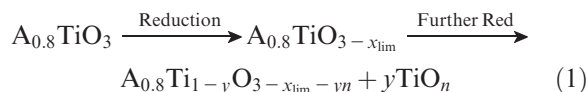
Figure 3. (a) XRD-reflection mode patterns performed on LST porous pellets (density (ρ_r) of ~63%) prereduced at 1100 °C (spectrum a), 1200 °C (spectrum b), and 1300 °C (spectrum c) for 10 h in 5% H_2/Ar. Asterisk symbols (∗) denote peaks from the aluminum holder. (b) Plot of the cell parameters of the samples described in panel (a) versus the reduction temperature; the increase in the cell parameter, relative to the starting value (air-sintered sample), is also shown. The errors are smaller than the symbols used for plotting.

Table 4. Microstructure of LST Pellets before and after Reduction

Before reduction (sintered in air)	After reduction at 900°C in PO₂ jig and testing for 1 week.	Detailed SEM image of the observed crystal growth on the main grains.

suggested by theoretical calculations for other perovskite system.[24] The exsolution occurs after an oxygen deficiency limit (x_{lim}) is reached:

$$A_{0.8}TiO_3 \xrightarrow{\text{Reduction}} A_{0.8}TiO_{3-x_{lim}} \xrightarrow{\text{Further Red}}$$

$$A_{0.8}Ti_{1-y}O_{3-x_{lim}-yn} + yTiO_n \qquad (1)$$

$$A_{0.8}Ti_{1-y}O_{3-x_{lim}-yn}$$
$$\equiv A_{0.8/(1-y)}TiO_{(3-x_{lim}-ny)/(1-y)} \qquad (2)$$

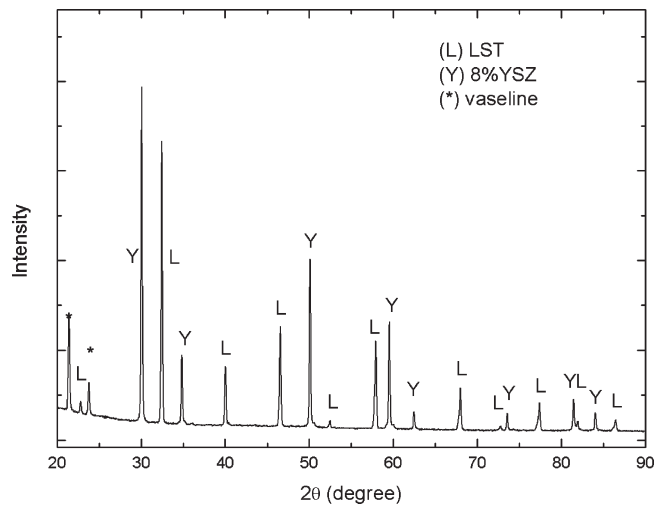(24) Islam, M. S.; Davies, R. A. *J. Mater. Chem.* **2004**, *14*, 86.

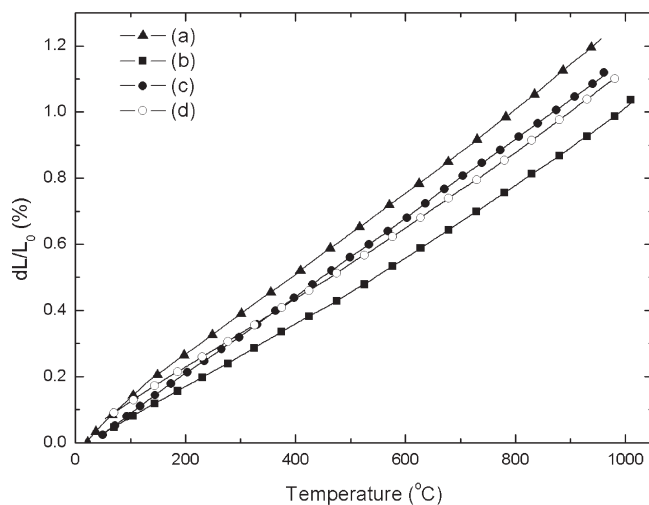**Figure 4.** XRD pattern of a fine mixture of 8YSZ and LST after firing at 1400 °C.

Figure 5. Thermal expansion coefficients measured from 50 °C to 1000 °C in air on pellets with $\rho_r \sim 70\%$ (a) and $\rho_r \sim 60\%$ (b); in 5% H_2/Ar, on cooling, on a pellet sintered in air, $\rho_r \sim 60\%$ (d) and on a pre-reduced pellet at 1050 °C, $\rho_r \sim 60\%$ (c).

3.3. Compatibility with the Electrolyte. It is important that no chemical reactions take place between the electrolyte and the anode material during operation of the cell. To confirm that no chemical interactions take place between LST and the usual electrolyte material, 8-mol%-yttria-stabilized zirconia (8YSZ), a fine mixture of the two materials was pressed into a pellet and fired for 12 h at 1400 °C. No secondary phase was observed in the XRD pattern performed on this mixture after firing. (See Figure 4.)

Equally important to the functioning of the cell is a good match between the thermal expansion coefficients (TECs) of LST and YSZ. Because the anode must be porous, only porous pellets have been tested (Figure 5). Table 5 gvies a list of the most relevant TEC values that have been measured. All of the TEC values are very close to the reported value of YSZ (TEC $\approx 1.05 \times 10^{-5}$ K^{-1}); therefore, good thermomechanical compatibility with YSZ should be expected in air or 5% H_2/Ar for pellets with 30%−40% porosity within the temperature range of 50−1000 °C.

Table 5. Thermal Expansion Coefficient (TEC) Values of Porous LST Pellets in Different Atmospheres

| | Conditions | | | |
TEC $(\times 10^5\,K^{-1})$	atmosphere	temperature range (°C)	relative density, ρ_r (%)	pellet history
1.035	air	50–1000	~60	sintered in air
1.297	air	50–1000	~70	sintered in air
1.189[a]	5% H$_2$/Ar	50–1000	~60	sintered in air
1.160	5% H$_2$/Ar	50–1000	~60	sintered in air and reduced at 1050 °C

[a] Measured upon cooling.
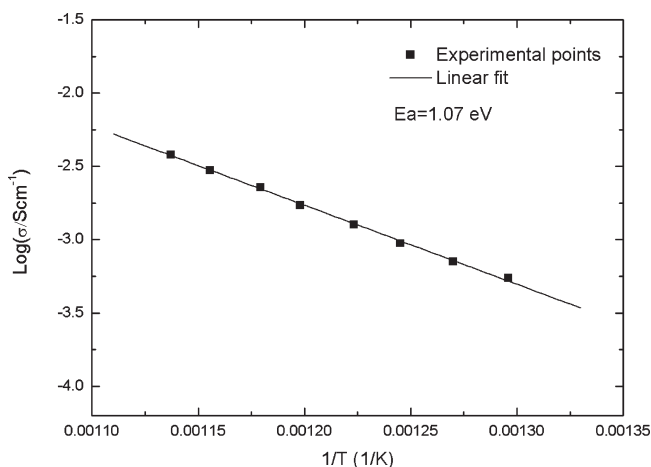
Figure 6. Arrhenius plot of the conductivity upon heating an LST porous pellet ($\rho_r \approx 60\%$, previously sintered in air) to 900 °C in air.

3.4. Electrical Properties. Because the anode of a SOFC must be porous, this study focused more on the properties of pellets with controlled porosity rather than on the properties of dense pellets. In the following four-probe conductivity experiments, a pellet having a relative density of ~65% was used. Upon heating in air, LST that has been sintered in air behaves like a semiconductor, reaching a conductivity of ~10^{-2} S cm^{-1} at 900 °C (see Figure 6). The activation energy for the conduction is rather high (1.07 eV).

At this point, a flow of 5% H$_2$/Ar was passed through the testing furnace, reducing the p_{O_2} value. In Figure 7, the response of the material, in terms of conductivity, upon this sudden change in p_{O_2}, is plotted against time. This plot shows that the conductivity of the material increases by ~2 orders of magnitude, within a matter of minutes, to ~0.3 S cm^{-1}. After this initial step, the conductivity continues to increase, but very slowly (see Figure 8). Approximately 15 h were needed for the material to increase its conductivity by another order of magnitude. The plot in Figure 8 also shows that the lower the p_{O_2} value, the higher the maximum (equilibrium) conductivity achieved. However, it is important to emphasize the slow increase in conductivity at constant p_{O_2} and temperature, which is in contrast to the initial jump in conductivity upon a decrease in p_{O_2}. One could therefore distinguish two main stages in the reduction of this material at a constant temperature: an initial stage, where the conductivity of the material increased very rapidly on
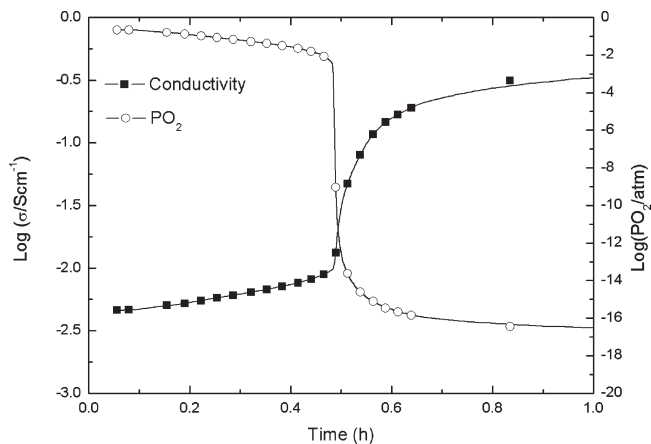
Figure 7. Conductivity and p_{O_2} versus time, at an early stage of the reduction of an LST pellet having 35% porosity at 900 °C.
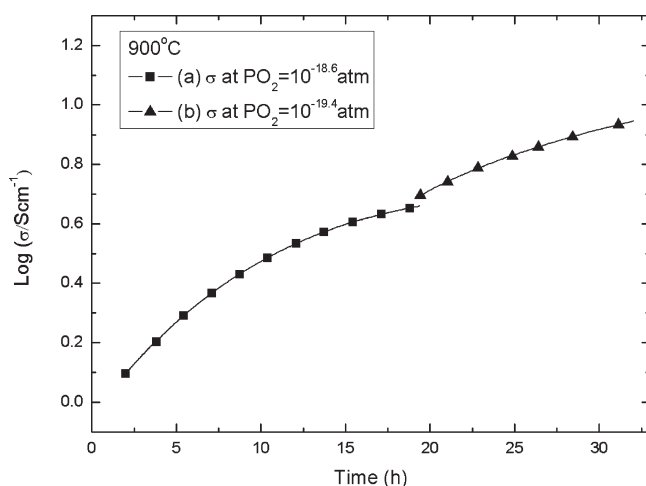
Figure 8. Conductivity versus time upon reduction of an LST pellet (35% porosity) at 900 °C: (a) data recorded just after the initial sudden change in p_{O_2}, when the p_{O_2} value stabilized to ~$10^{-18.6}$ atm; and (b) data recorded after cooling and reheating in 5% H$_2$/Ar, after the p_{O_2} value had stabilized at $10^{-19.4}$ atm.

switching to reducing atmosphere, and a second one, in which the conductivity increased very slowly with time, at constant p_{O_2}. This approach provides us with an interesting insight into the properties of this material. Previous studies have shown that the conductivity of this material is due to the Ti^{4+} ions reducing to Ti^{3+}, which is accompanied by the formation of oxygen vacancies (eq 3):[13]

$$2Ti_{Ti}^x + O_O^x \leftrightarrow 2Ti_{Ti}' + V_O^{\bullet\bullet} + \frac{1}{2}O_2 \qquad (3)$$
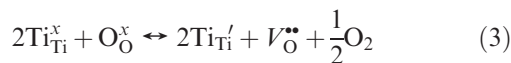
The material will exhibit metallic-type conductivity when the electron concentration increases sufficiently. Therefore, the conductivity will mainly depend on the extent of the reduction, which is determined by the concentration of the oxygen vacancies. The fact that the conductivity of the material increases rapidly when exposed to a reducing atmosphere suggests that the surface reaction between the gas phase and the grain surface is very fast at this temperature (900 °C), and, thus, a thin film of reduced material covers the surface of the grains rapidly. This thin film of reduced—and, thus, conductive—material provides a first flow path for the electrons, accounting for the initial
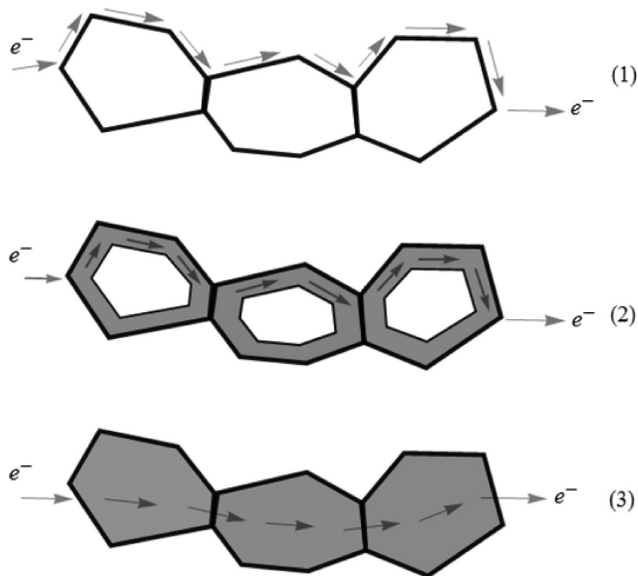
Figure 9. Schematic view of the proposed mechanism for the reduction of LST ceramics at high temperatures, at a given p_{O_2} value. (1) In the first stage, a layer of reduced material covers the surface of the grains, because of fast reaction between the gas phase and the solid surface. This layer provides a first flow path for the electrons, accounting for the initial jump in conductivity immediately after the decrease in p_{O_2}. (2) Gradually, the oxygen vacancies start diffusing into the bulk, increasing the thickness of the reduced layer that covers the grains. The flow path available to the electrons broadens and conductivity slowly increases. (3) The reduction process proceeds until the bulk of the grains has been reduced completely. The conductivity reaches a stable plateau and does not increase further.

Figure 10. Conductivity and p_{O_2}, as a function of time during a redox cycle performed on LST pellets at (a) 900 °C and (b) 670 °C. The pellets used (35% porosity) were previously prereduced in 5% H_2/Ar at 1100 °C for 10 h.

rapid initial increase of the conductivity. However, this also implies that the grain-boundary regions are subject to the same fast reduction upon atmosphere change, acting also as fast conduction paths and not as blocking features. In the second step, the reduction process will continue via the further removal of oxygen anions from the bulk of the grains. This is equivalent to the vacancies diffusing into the bulk. Gradually, the thickness of the reduced layer of the phase will increase, providing the electrons with wider flow paths, and making the material more conductive. Similar to most of the diffusion processes that take place in the bulk of the grains, this will be a very slow and difficult process, mainly dependent upon temperature and time. The reduction of the material slowly progresses until the entire grain has been reduced. A schematic view of the proposed mechanism is presented in Figure 9. A similar behavior has been reported and interpreted in a similar manner for yttrium-doped strontium titanate.[15]

The redox behavior of the reduced pellets has also been investigated. In Figure 10, the conductivity is plotted against time, upon oxidation followed by reduction at 900 °C (Figure 10a) and 670 °C (Figure 10b). The pellets employed in this example have ∼35% porosity and were previously reduced in 5% H_2/Ar at 1100 °C for 10 h. The conductivity loss associated with the oxidation process strongly depends on the oxidation temperature. The sample exposed to air at 900 °C needed only 2 h to decrease its conductivity to ∼10^{-2} S cm^{-1}, whereas the sample oxidized at 670 °C needed 12 h to reach the same value. It can therefore be assumed that the oxidation process takes place in reverse, compared to the reduction process. In the
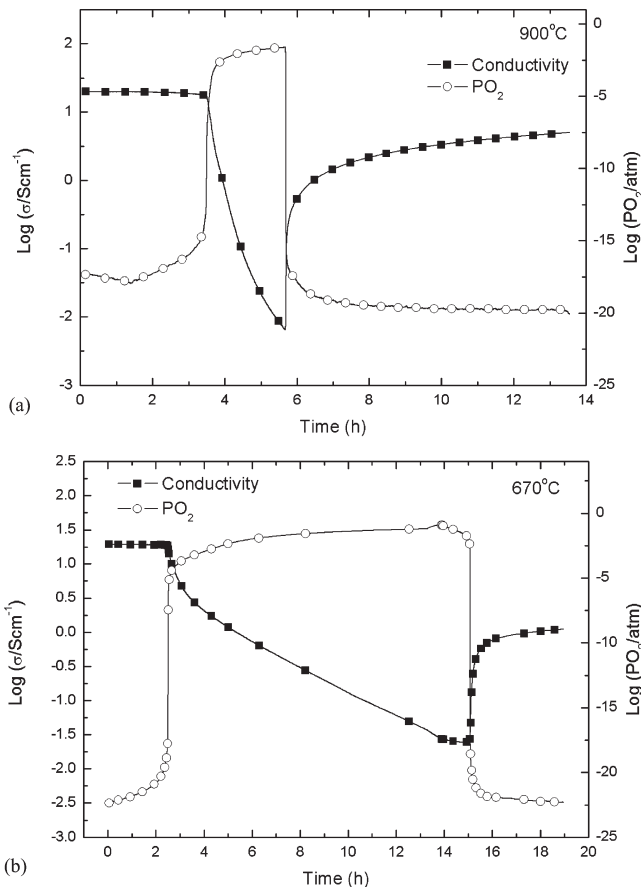
first stage, the surface of the grains will be oxidized. Depending on the surface exchange coefficient and the bulk diffusion coefficient of the oxygen at the oxidation temperature, the oxidation will proceed at different rates. The oxygen ions will gradually reoccupy the vacant atomic position in the oxygen sublattice, causing the oxidation of Ti^{3+} ions and thus reducing the conductivity. When the atmosphere was changed back to low p_{O_2}, the same fast initial response was noted for both temperatures (see Figure 10). It was, however, surprising to find that the material exhibited this type of behavior at the lower temperature of 670 °C. This finding suggests surface reactivity and conductivity are still very good at this temperature. It is also interesting to note that the conductivity of both samples is >1 S cm^{-1}, just after the initial stage, suggesting that a fraction of the bulk has not been oxidized. If all the bulk would have been oxidized, then the conductivity value should have been ∼0.3 S cm^{-1}, as reported in the first reduction experiment discussed (recall Figure 7). As expected, recovering the initial conductivity of the samples is strongly hindered by the slow bulk reduction kinetics, as can be seen in Figure 11.

It is also important not to neglect the influence of the microstructure on the redox behavior of the material. A microstructure with relatively large grains will have a higher probability of the grain core being still reduced after the material has been exposed to air. The microstructure
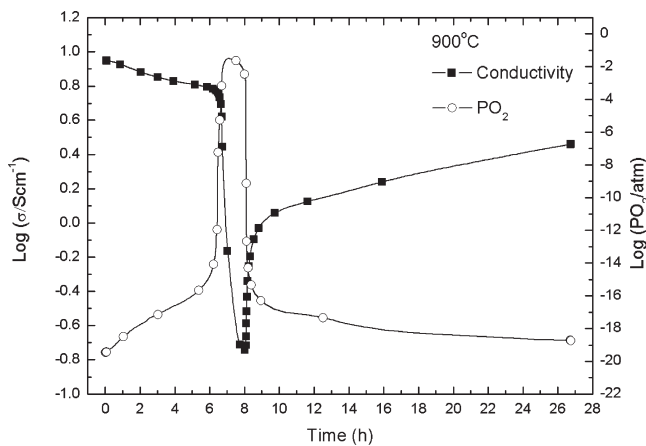
Figure 11. Oxidation followed by reduction for a porous LST pellet (35% porosity), at 900 °C. Conductivity and p_{O_2} data are plotted versus time. The pellet had been previously reduced in the testing jig, at 900 °C (20 h) in 5% H_2/Ar.
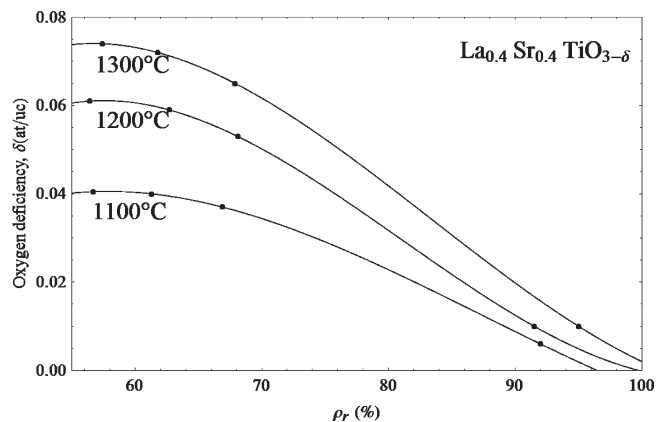

Figure 12. Oxygen deficiency versus relative density for porous and dense pellets prereduced at different temperatures (1100, 1200, and 1300 °C) for 10 h, under continuous 5% H_2/Ar flow.

of the pellets employed in this experiment had microstructures similar to those presented in Table 4.

This interpretation of the observed behavior leads to some consequences. First, the fact that the surface of the material is so reactive and can become readily conductive suggests that it can have good catalytic properties and possess the appropriate sites to promote electrochemical reactions. Second, the bulk diffusion of the oxygen vacancies seems to be the rate-determining process in achieving conductivities in excess of 0.5 S cm^{-1} in a shorter time. Bulk diffusion could be enhanced either by performing the reduction at higher temperatures or by increasing the oxygen anions mobility via doping. The first approach will be presented in the remainder of this paper.

A simple experiment was used to study the influence of the porosity and reduction temperature on the extent of the reduction and conductivity. LST pellets with relative densities of ~57%, ~63%, and ~68% with controlled microstructure were prepared by sintering in air. Their weight was recorded before and after a reduction process that was carried out in a tubular furnace, in a continuous 5% H_2/Ar flow at 1100, 1200, and 1300 °C for 10 h. It is generally accepted that, in this material, conduction takes place because of the reduction of the Ti^{4+} ions associated with oxygen loss[13] (eq 3). Assuming that only oxygen loss is responsible for the weight loss, the following equation can be derived:

$$\Delta = \frac{m_i - m_f}{m_i} = \frac{A_O(\delta - \delta_0)}{\mu_{LST} - A_O\delta_0} \qquad (4)$$

If there is no significant oxygen deficiency that contributes to conduction before the reduction process, meaning that the sample has been prepared in air, its conductivity is ~10^{-2}–10^{-3} S cm^{-1}; then,

$$\delta_O \ll \delta \Rightarrow \delta = \frac{\mu_{LST}}{A_O} \qquad (5)$$

where Δ is the weight loss of the pellet, m_i the initial mass of the pellet (before reduction), m_f the mass of the pellet

Table 6. Conductivity of Prereduced LST Pellets of Different Relative Densities Measured at 880 °C in 5% H_2/Ar

| relative density, ρ_r (%) | Conductivity after Prereduction (S cm^{-1}) | | | Measurement Conditions | |
	@ 1100 °C	@ 1200 °C	@ 1300 °C	temperature (°C)	technique
68	17	28	44	880	four-probe
63	18	31	40	880	Van der Pauw
57	16	20	32	880	four-probe

after reduction; δ_0 the oxygen deficiency per formula unit before reduction ($La_{0.4}Sr_{0.4}TiO_{3-\delta_0}$), δ the oxygen deficiency per formula unit after reduction ($La_{0.4}Sr_{0.4}TiO_{3-\delta}$), and A_O the atomic weight of oxygen.

Using eq 5, the oxygen deficiency for the reduced pellets was calculated. The result is presented in Figure 12. The experimental points (shown on this plot as points) were used to create interpolating curves. The plot shows clearly that the higher the reduction temperature, the higher the oxygen loss. However, a very important effect on the oxygen loss is due to the porosity of the samples. The porous pellets are easier to reduce due to the higher contact surface between the gas phase and material and due to shorter diffusion distances. The samples with higher relative densities show the same difficult oxygen diffusion suggested by the conductivity measurements.

The conductivity of some of these pellets was also measured and found to be strongly influenced by the porosity and prereduction temperature. A list of these conductivities is given in Table 6. For a given porosity, the conductivity increases with the increase of the prereduction temperature. Conductivities of up to 44 S cm^{-1} for samples having 68% relative density have been measured at 880 °C, in 5% H_2/Ar. The effect of the porosity on the conductivity becomes more important as the extent of the reduction of the material increases. For example, for the pellets prereduced at 1100 °C when increasing the relative density from 57% to 68%, the conductivity increases from 16 to 17 S cm^{-1}, respectively. However, when considering pellets prereduced at a higher temperature (for example, 1200 °C), the increase is from 20 S cm^{-1} to 28 S cm^{-1}, for the same increase in relative density.
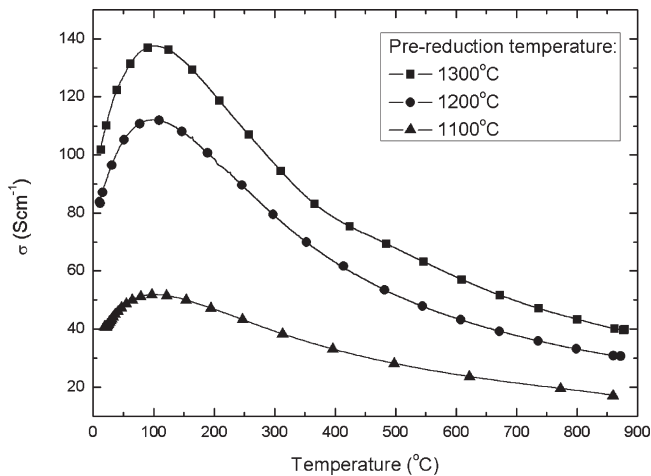
Figure 13. Conductivity versus temperature for pellets having a relative density of 63%, prereduced at 1100, 1200, and 1300 °C, measured in 5% H_2/Ar.
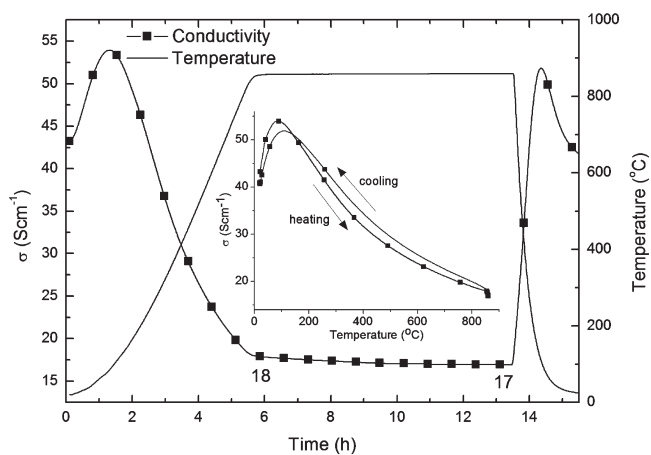

Figure 14. Conductivity against time for a porous prereduced pellet, showing the degradation of the electrical properties when the p_{O_2} is $> 10^{-19}$ atm at 880 °C. The inset plot represents the temperature dependence of the thermal history shown on the main axes.

The form of the $\sigma(T)$ dependences also deserves some attention. It can be seen from Figure 13 that the samples present a peak in conductivity at ~100 °C. Similar behavior was previously observed for some lanthanum-doped strontium titanate ceramics, but not for the single crystals as well, suggesting electron trapping at grain boundaries.[25] After this peak, the conductivity decreases quickly with increasing temperature, indicating a metallic behavior. This decrease in conductivity becomes more significant as the prereduction temperature increases.

Of course, it is interesting to see whether these conductivities can be maintained for a long period of time. Surprisingly, the electrical properties do not seem to degrade in time, but rather to improve slightly if the p_{O_2} is extremely low. Figure 14 shows a slow decrease of the conductivity at 880 °C when the p_{O_2} value is higher than ~10^{-19} atm. However, if the p_{O_2} value is $< 10^{-20}-10^{-21}$ atm, the conductivity increases slightly at high temperatures and more significantly at temperatures lower than

(25) Moos, R.; Hardtl, K. H. *J. Appl. Phys.* **1996**, *80*, 393–400.
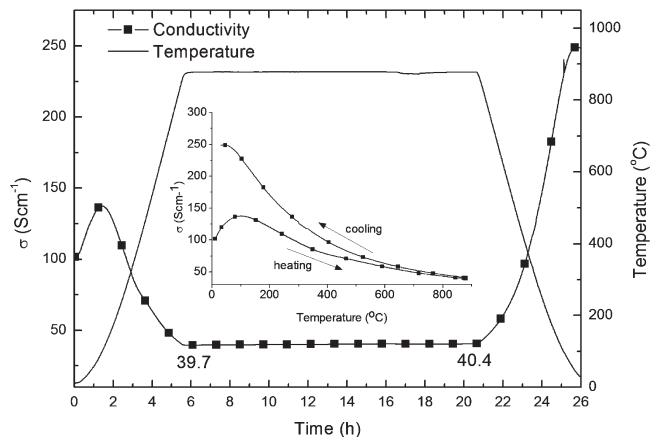

Figure 15. Conductivity versus time and temperature profile for a pre-reduced porous sample, showing the improvement of electrical properties when kept at 880 °C and $p_{O_2} < 10^{-20.5}$ atm. The inset plot represents the temperature dependence of the thermal history shown on the main axes.
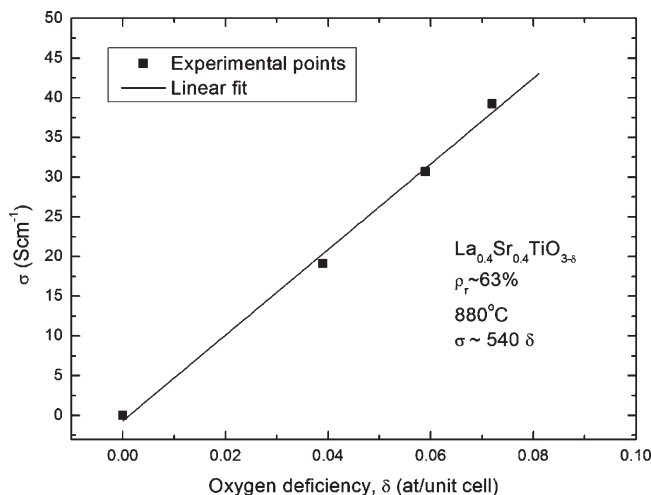

Figure 16. Conductivity versus oxygen deficiency for pellets with a relative density of $\rho_r \sim 63\%$, measured at 880 °C in 5% H_2/Ar. The pellets have been prereduced at different temperatures and thus possess different oxygen deficiency. A linear dependence is observed between the σ and δ. The errors are smaller than the points.

350−400 °C (Figure 15, inset graph). This is more likely to be due to a decrease of the grain-boundary resistance rather than a further bulk reduction of the material.

By plotting the conductivity of pellets with similar porosity against oxygen deficiency, a linear dependence was found (see Figure 16). As expected, the conductivity increases with the oxygen deficiency. Because the difference in cell parameter between the three samples is not significant, the charge concentration should be proportional to the oxygen deficiency, assuming all the electrons produced by oxygen loss are free electrons. Having in mind that $\sigma = ne\mu$, this plot suggests that the conductivity increase is due to an increase in the concentration of the charge carriers, the electrons in samples having very similar mobility in the three pellets.

To get an idea about the maximum conductivity achievable for this compound, a dense sample was sintered in 5% H_2/Ar for 12 h, at 1400 °C. The conductivity of the dense pellet was measured and the results are plotted
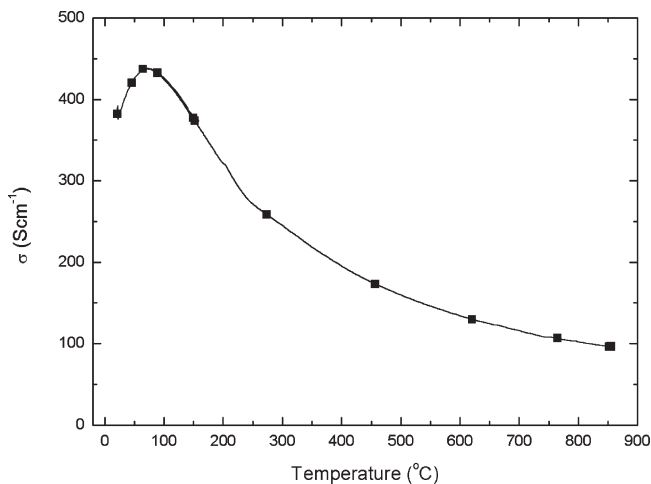
Figure 17. Conductivity versus temperature for a LST dense sample sintered in 5% H_2/Ar for 12 h.

Figure 18. Calculated conductivity as a function of relative density (ρ_r) for pellets reduced at different temperatures for a given time. The plot combines the effect of the porosity on the reduction of the material and on the conduction.

versus temperature in Figure 17. The curve shows the same evolution as the prereduced samples, with a strong drop of the conductivity versus temperature. However, the conductivity is significantly higher at 880 °C, reaching a value of ~96 S cm^{-1}.

If we consider the experiments presented above, where the samples sintered in air have been prereduced at high temperatures, then it becomes clear that, in this situation, the conductivity of the material is mainly dependent on two parameters: the extent of the reduction and the porosity. The extent of the reduction is a direct measure of the intrinsic conductivity of the material, while the porosity affects conduction in the ceramic body. However, the extent of the reduction is not actually an independent variable either, because, for a given material, reduction time, and temperature, it depends on the porosity (recall Figure 12). Therefore, there are two antagonistic effects of the porosity on the conductivity on reduction of a pellet with a given microstructure, at a given temperature and for a given duration. A higher porosity will favor a higher extent of the reduction; however, at the same time, a higher porosity will decrease the conductivity of the material. Thus, a balance between the two effects should be identified, that would correspond to the optimum porosity that will provide the highest conductivity. A very simplified way of describing this anticipated behavior is presented in the equations below.

The conductivity will be given by

$$\sigma(\delta, \rho_r) = k\delta\rho_r \qquad (6)$$

where k is a constant and ρ_r is the relative density.

From Figure 12, the oxygen deficiency can be described by a polynomial, for $\rho_r > 0.5$:

$$\delta(\rho_r) = a_0 + a_1\rho_r + a_2\rho_r^2 + a_3\rho_r^3 \qquad (7)$$

The conductivity will then be a function of relative density only:

$$\sigma(\rho_r) = k(a_0 + a_1\rho_r + a_2\rho_r^2 + a_3\rho_r^3)\rho_r \qquad (8)$$

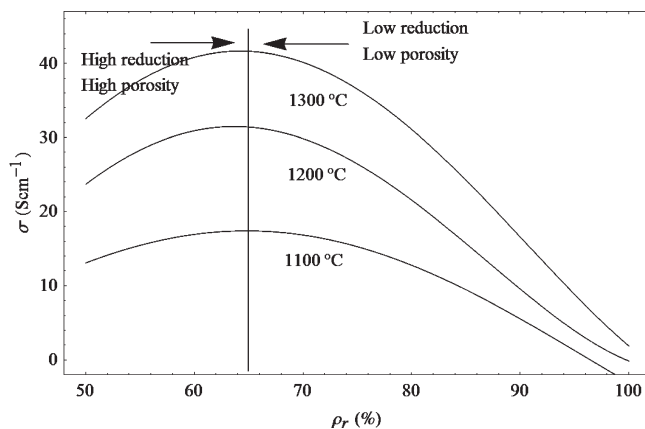As expected, Figure 18 shows that there is an optimum porosity that favors a good reduction and sufficient connectivity between grains so that, for a given temperature and duration of the reduction, the conductivity will be maximum. Also, the maximum gets narrower as the prereduction temperature increases. These facts should be considered when evaluating the reduction rate of a material in a specified duration, because one might not only compare samples with different porosity but also with different extents of reduction.

3.5. TGA Studies. To further investigate the mechanism for the reduction of LST ceramics, TGA analysis was used. Two powder samples of different specific surface area were used: 0.035 m^2/g and 0.384 m^2/g. The coarse powder was prepared by crushing a dense LST pellet in a mortar, consisting mainly of particles with diameters between 1 mm and 50 μm. The specific surface area should be similar to the specific surface area of pellets with a relative density of 55%−65%. The fine powder was prepared from the previous one by ball milling for 4 h. The particle size was, on average, < 20 μm. The samples were heated in a 5% H_2/Ar flow to 1000, 1100, 1200, and 1300 °C, with a dwell time of 4 h at each temperature step (see Figure 19a).

As can be seen from Table 7, the weight loss after 4 h at 900 °C is very small, even for the fine powder. This shows how slow the bulk diffusion/surface exchange is in this material, at this temperature. At higher temperatures, the weight loss becomes easily detectable, exceeding the detection limit of the instrument and providing consistent data. Also, it is interesting to note that the oxygen deficiency achieved is preserved upon cooling ("frozen"). This might be due to the relatively high cooling rate, but some of our experiments point out that, even for usual cooling rates (such as 5 °C/min), this still holds true. In Figure 19b, the oxygen deficiency per temperature step is plotted for each temperature. The plot shows that the rate of the weight loss (increase of the deficiency) reaches a plateau after 1200−1300 °C, suggesting the material reaches a limit for the rate of extraction of the oxygen from its structure.

The data recorded for each temperature step were fitted using a kinetic model from the literature[26] that should

(26) McColm, T. D.; Irvine, J. T. S. *Solid State Ionics* **2002**, *152−153*, 615–623.
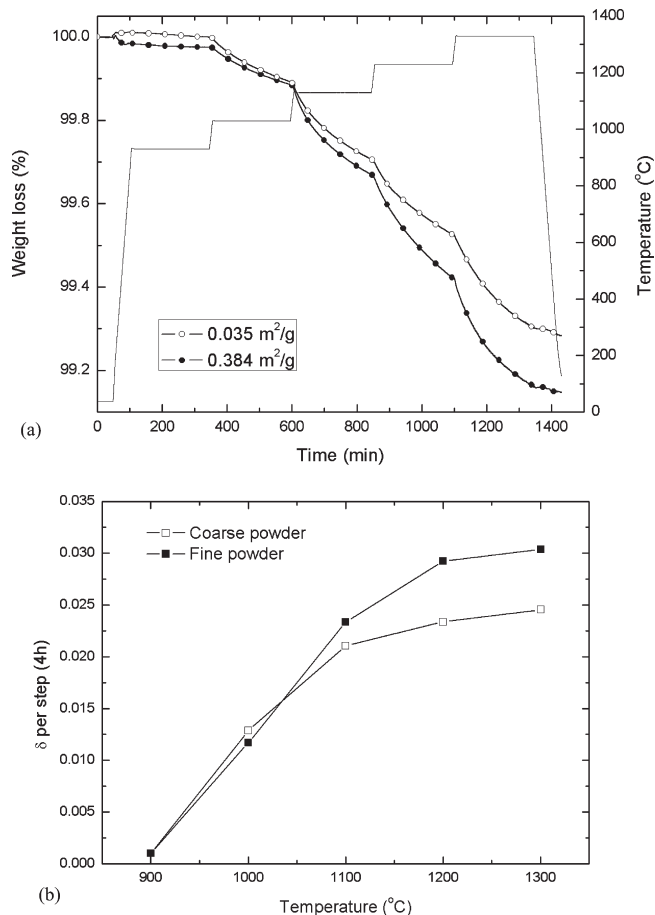
Figure 19. (a) TGA analysis performed on LST powders with different specific surface areas. The data were collected at isothermal steps of 4 h at 900, 1000, 1100, 1200, and 1300 °C, under a 5% H_2/Ar flow. (b) Oxygen deficiency reached per temperature step against reduction temperature for the two powders analyzed by TGA.

Table 7. Cumulated Weight Loss and Calculated Oxygen Deficiency for the TGA Analysis of Two LST Powders (0.035 and 0.384 m²/g)

temperature (°C)	Cumulative Weight Loss (%)		Cumulative δ (at/uc)	
	coarse powder	fine powder	coarse powder	fine powder
900	0.01	0.01	0.001	0.001
1000	0.12	0.10	0.014	0.012
1100	0.30	0.31	0.035	0.036
1200	0.50	0.56	0.059	0.065
1300	0.71	0.82	0.083	0.096

reflect the kinetics of the two proposed processes, described by the two exponentials:

$$m(t) = k_0 + k_1 e^{-k_2 t} + k_3 e^{-k_4 t} \qquad (9)$$

The regression plot showed that the data can be fitted very well by the proposed equation. The regression curves suggest that the minimum time required for these samples to achieve equilibrium above 1100 °C is 10 h (see Figure 20). The time constants confirm that one of the processes is fast and one is slow ($k_2 > k_4$), and also that the latter has the higher contribution on the weight loss ($k_3 > k_1$), as suggested previously based on the reduction mechanism derived from conductivity data (see Table 8). This holds true for all calculated regressions at each temperature
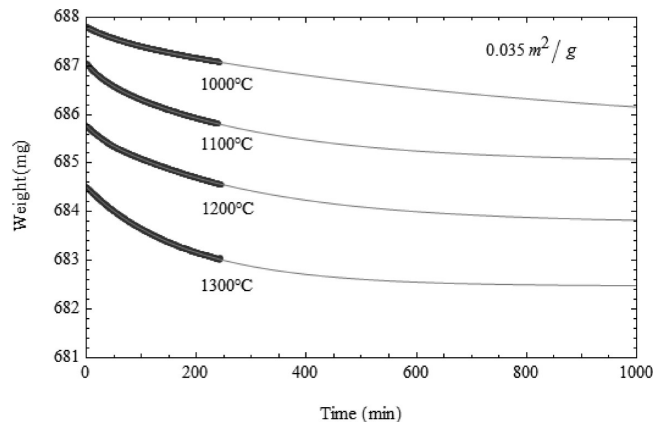

Figure 20. Experimental data (points) and regression fit (continuous line) for the TGA analysis of coarse LST powder.

Table 8. Fitting Parameters for Two of the Fitting Curves Presented in Figure 20

temperature (°C)	k_1 (mg)	k_2 (mg)	k_3 (min^{-1})	k_4 (mg)	k_5 (min^{-1})
1000	685.526	0.20907	0.01633	2.06637	0.00119
1100	685.018	0.24691	0.03114	1.78939	0.00341
1200	682.346	0.29390	0.02653	3.13730	0.00143
1300	682.466	0.07701	0.01892	1.96929	0.00523

step. However, interpreting the values of the regression parameters, in relation to the corresponding temperatures, is more difficult, because of the fact that the samples did not reach equilibrium at the isothermal steps.

XRD analysis has been performed on the reduced powders to check if they preserved their crystal structure after such an extended exposure to reducing atmosphere at high temperatures. Both of the powders did not show any extra peak on the spectrum. However, it does seem remarkable that the perovskite structure can accommodate an A-site deficiency of 0.2 and an oxygen deficiency of almost 0.1.

The cell parameters at different extents of reduction have been investigated (see Figure 21). The oxygen deficiency, as derived in eq 4, was used as a measure of the extent of the reduction, and, similar to powder XRD, is an average property of the material. As expected, the cell parameter increases with the extent of the reduction, as explained earlier.

Previously, an empirical equation for the prediction of the cell parameters based on the Shannon radii[27] has been proposed for fluorite materials:[28]

$$a = a_0 + \sum_k x_k (b_0 \Delta r_k + b_1 \Delta z_k) \qquad (10)$$

where a is the cell parameter; a_0, b_0, and b_1 are constants; x_k is the mole fraction of the cation k substituting for the host cation; Δr_k is the difference in the ionic radius between the substituting cation k and the host; and Δz_k is the difference in charge between the substituting cation

(27) Shannon, R. D. *Acta Crystallogr., Sect. A: Cryst., Phys., Diffr., Theor. Gen. Crystallogr.* **1976**, *32*, 751–767.
(28) Kim, D. *J. Am. Ceram. Soc.* **1989**, *72*, 1415–1421.

Article

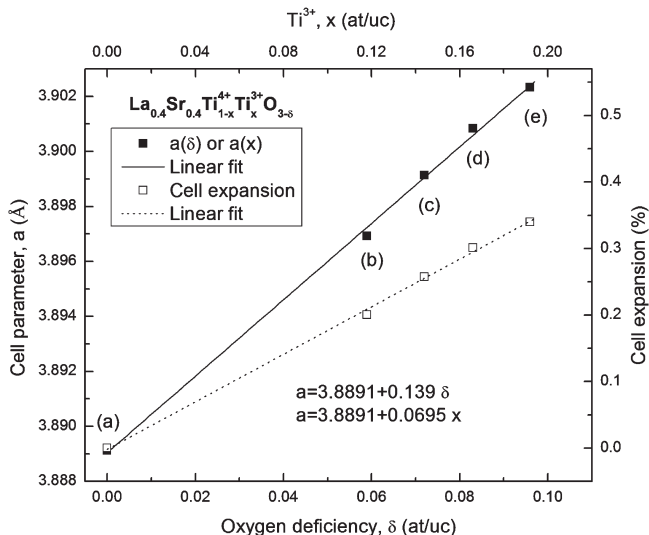*Chem. Mater., Vol. 22, No. 17, 2010* 5053

Figure 21. Plot showing the cell parameter against oxygen deficiency for different samples: (a) sintered in air; (b) prereduced at 1200 °C for 10 h, $\rho_r \approx 63\%$; (c) prereduced at 1300 °C for 10 h, $\rho_r \approx 63\%$; (d) the coarse powder used in the TGA tests; (e) the fine powder used in the TGA tests. The errors are smaller than the points.

k and the host cation. To the best of our knowledge, the validity of this equation for perovskites has not yet been proven. We have found that this equation works well at least for cubic perovskites, with the coefficients $b_0 = 1$ and $b_1 = 0.002$. For the substitution of Ti^{4+} by Ti^{3+}, this equation becomes

$$a = a_0 + x_{Ti^{3+}}[r_{Ti^{3+}} - x_{Ti^{4+}} + 0.002(-1)]$$

or, using the Shannon radii (NC = 6),

$$a = a_0 + 0.063 x_{Ti^{3+}}$$

The value of the slope in the equation above (0.063) is extremely close to that determined experimentally (0.069) and shown in Figure 21. This suggests that the main reason for the expansion of the unit cell of this titanate upon reduction is the formation of the Ti^{3+} ion, which is larger than the host cation, Ti^{4+}. However, the predicted slope is slightly smaller than the experimentally determined one, suggesting that there is some expansion that the Ti^{3+} substitution does not account for. Most likely, this expansion is due to the formation of the oxygen vacancies that accompanies the reduction process.

4. Conclusions

$La_{0.4}Sr_{0.4}TiO_3$ (LST) ceramics have been investigated to establish their potential application as anode materials in solid oxide fuel cells (SOFCs). The material has been shown to form a primitive-type cubic structure when sintered either in air or under strongly reducing conditions. The samples sintered in air have semiconductor-type behavior, reaching a conductivity of $\sim 10^{-3}$ S cm^{-1} at 900 °C, whereas the sample sintered in 5% H_2/Ar shows metallic-type behavior, with a conductivity of $\sim 10^2$ S cm^{-1} at the same temperature and $p_{O_2} \approx 10^{-20}$ atm. The conductivity of the samples prepared in air can be increased by prereduction at high temperatures, reaching a conductivity of ~ 44 S cm^{-1} at 900 °C for a sample with 32% porosity. X-ray diffraction (XRD) patterns taken after reduction at high temperatures do not show any change in the symmetry of the material or formation of a secondary phase. However, microstructural studies suggest a secondary phase consisting of submicrometer crystals might develop on the main grains. The conductivity of the prereduced pellets has been shown to increase linearly with the oxygen deficiency. Thermogravimetric analysis (TGA) analysis and conductivity experiments have indicated that LST ceramics have a fast initial response to atmosphere-type changes, rapidly increasing or decreasing its conductivity; however, the completion of the reduction process is much slower. It seems likely that the limiting process responsible for achieving conductivities above 0.5−1 S cm^{-1} is the diffusion of oxygen vacancies through the bulk of the grains.

LST does not react with the usual choice of electrolyte material, yttria-stabilized zirconia (YSZ), even at elevated temperatures. Moreover, the thermal expansion coefficients of the two materials are similar either in air or a 5% H_2/Ar environment.

An equation that relates the size of the B-site ions with the cell parameter has been adapted from the literature. The equation accounts well for the expansion of the cell on reduction and suggests that this expansion is mainly due to the increased size of the Ti^{3+} ions, compared to the Ti^{4+} ions.